Tailoring ZnO nanostructures for transparent photodetector applications in hybrid liquid crystals

Claire Legrain[1], Margot Dhennin[1], Carine Davoisne[2], Nicolas Brouckaert[3], Nina Podoliak[3], Malgosia Kaczmarek[3], Sébastien Saitzek[1], Jean-François Blach[1,]*

1 Univ. Artois, CNRS, Centrale Lille, Univ. Lille, UMR 8181, Unité de Catalyse et Chimie du Solide (UCCS), F-62300 Lens, France

2 Laboratoire réactivité et chimie des solides (LRCS), CNRS-UMR 6007, Université de Picardie Jules Verne, 33 Rue Saint Leu, 80039 Amiens Cedex, France.

3 School of Physics and Astronomy, Southampton S017 1BJ, United Kingdom

*** Corresponding author : jfrancois.blach@univ-artois.fr**

ABSTRACT

We report on enhancing the electro-optical response of nematic liquid crystal (6CHBT) by doping with increasing concentration of ZnO nanoparticles. Photosensitive response of this hybrid system is shown through the generation of a photocurrent at 450 nm. The critical role of surfactants to ensure uniform dispersion of nanoparticles in the liquid crystal matrix, and their interplay with the charge carrier collection process, are also demonstrated. Such properties allow these hybrid liquid crystals to be used in the design of photodetectors, integrated into liquid crystal displays, without compromising their transparency.

GRAPHICAL ABSTRACT :

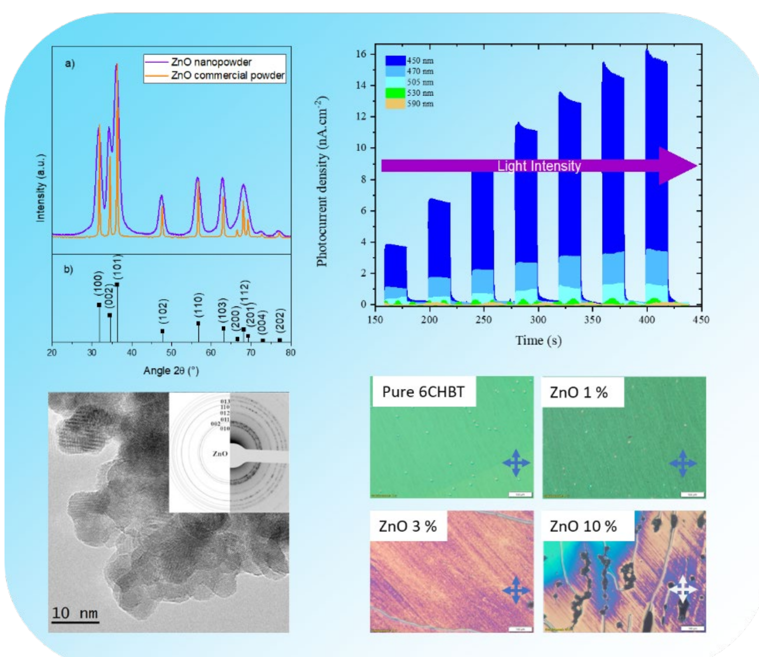

KEYWORDS :

Nematic liquid crystals, ZnO nanoparticles, Photoelectrochemistry, Photodetector

1. INTRODUCTION

The realm of light detection technology, particularly within the domain of ultraviolet (UV) or visible (VIS) detection, requires innovative solutions for the applications requiring thin film format or integration with other optical materials. The range of such applications covers a wide range of fields such as space-based communication [1], combustion monitoring [2], ozone level surveillance [3], photovoltaic cells [4] and phototransistor devices [5]. Several semiconductor materials were harnessed for photodetectors applications, such as Gallium Nitride (GaN) [6], Titanium Dioxide (TiO_2) [7], Diamond [8] and Silicon Carbide (SiC) [9]. Among these materials Zinc Oxide (ZnO) [10] attracted significant attention due to its wide band gap and attractive properties in terms of both chemical composition and thermal resilience. In addition, ZnO [11] has been observed to exhibit relatively strong photoconductivity and high transparency in the visible spectrum, allowing its application as transparent electrode in solar cell[12]. The second type of optical material used in this investigation, namely liquid crystals, found extensive use in fields such as displays [13], sensors [14], and solar cells [15]. Liquid crystals exhibit an interesting state of matter which combines the fluidity of liquids with the ordered structure of crystals, allowing precise control over optical (birefringence)[16] and electrical (electrical anisotropy)[16] properties. Furthermore, the integration of dielectric nanoparticles into liquid crystal matrices has shown considerable potential for tuning and enhancing the optical [17–19] and electrical properties [20–22] of the resulting hybrid systems. Zinc oxide nanoparticles, characterized by their unique semiconducting and optoelectronic properties, have emerged as a significant candidate for such hybrid systems. Embedding a photodetector directly within a liquid crystal display offers an intriguing opportunity to create an integrated sensor for mobile applications.

This work explores the impact of ZnO nanoparticles dispersion interactions within a nematic liquid crystal matrix and determines the photoresponse of such systems. First, the microstructural, morphological and optical properties of ZnO nanoparticles are described. Then, ZnO nanoparticles (NPs) suspensions within a 6CHBT liquid crystal matrix are demonstrated, and their influence on the liquid crystal electro-optical properties, along with the photocurrent transition responses of the system, are studied via photoelectrochemical measurements.

2. MATERIALS AND METHODS

Synthesis of ZnO nanoparticles :

ZnO NPs were synthesized based on the method described by L. Spanhel et *al.* [23,24]. Firstly, a 5 mmol solution of Zinc acetate dihydrate ($Zn(OAc)_2.2H_2O$, Sigma Aldrich,) is dissolved in 50 mL of absolute ethanol(CH_3CH_2OH, Sigma Aldrich). This solution is then placed in a reflux assembly then heated at 80°C for 1 hour under atmospheric pressure until a translucent solution is obtained. In parallel, a 11 mmol basic solution of $LiOH.H_2O$ (Sigma Aldrich, ≥99,0 %) is prepared in absolute ethanol (Ultrasound can be used to facilitate dissolution). After cooling the solution containing the Zn precursor to room temperature, the basic solution is added dropwise and with vigorous stirring. The precipitate formed is recovered by centrifugation (10 min, 3500 rpm), then washed twice with ethanol, 95% and finally dried at 90°C for 1 h to obtain a whitish ZnO powder. The influence of lithium ions makes it possible to limit the size of the crystallites and generally leads to the formation of spherical particles [25,26].

The structural characterization was investigated using a Rigaku ULTIMA IV diffractometer using the K-alpha radiation of Cu (1.54184 Å). XRD patterns are recorded in the classic Bragg-Brentano geometry in the range 20° to 80° with step size of 0.02° and a speed of $0.3°min^{-1}$.

The photoelectrochemical measurements were performed using a PGSTAT204 potentiostat/galvanostat (Metrohm) equipped with the Electrochemical Impedance Spectroscopy (EIS) module and coupled with optical bench (LED Driver Kit, Metrohm) consisting of LED sources (450, 470, 505, 590, and 627 nm) with low spectral dispersion. The power density of the light can be controlled by a photodiode and controlled using NOVA 2.0 software. A two-electrode configuration was used for the measurements on the cells.

Transmission Electron Microscopy and selected area electron diffraction (TEM, FEI Tecnai F20 STWIN) were employed for investigation of the microstructure, grain size and crystallinity of the nanoparticles.

3. RESULTS AND DISCUSSION

3.1 ZnO Nanopowder characterization

For this study, ZnO nanopowder was synthesized via a method described in the materials and methods section. In order to ensure the powder purity, XRD measurements were carried out on the synthesised powder and a commercially available one (from Strem Chemicals). We note that all diffraction peaks of this powder are situated at theoretically predicted position of wurtzite ZnO and that we do not observe peaks attributed to another material. We can therefore conclude that this powder is composed of pure ZnO. In addition, we note a large broadening of all peaks by comparison to the diffractogram recorded on the commercial ZnO powder, indicating that the average crystallite size of our powder is notably small. Moreover, in the case where micro-strains are neglected, it is well established that the estimation of average crystallite size can be achieved through the application of Scherrer's law[27] $D = \frac{K\lambda}{\text{FWHMs } cos\theta}$,where λ is the X-ray wavelength (λK_α(Cu) = 1.5418 Å), FWHMs corresponds to the broadening induced by the size effect which is deconvolved from the instrumental part, K is a dimensionless shape factor (with a typical value of 0.89) and θ is Bragg's angle corresponding to (hkl) reflection.

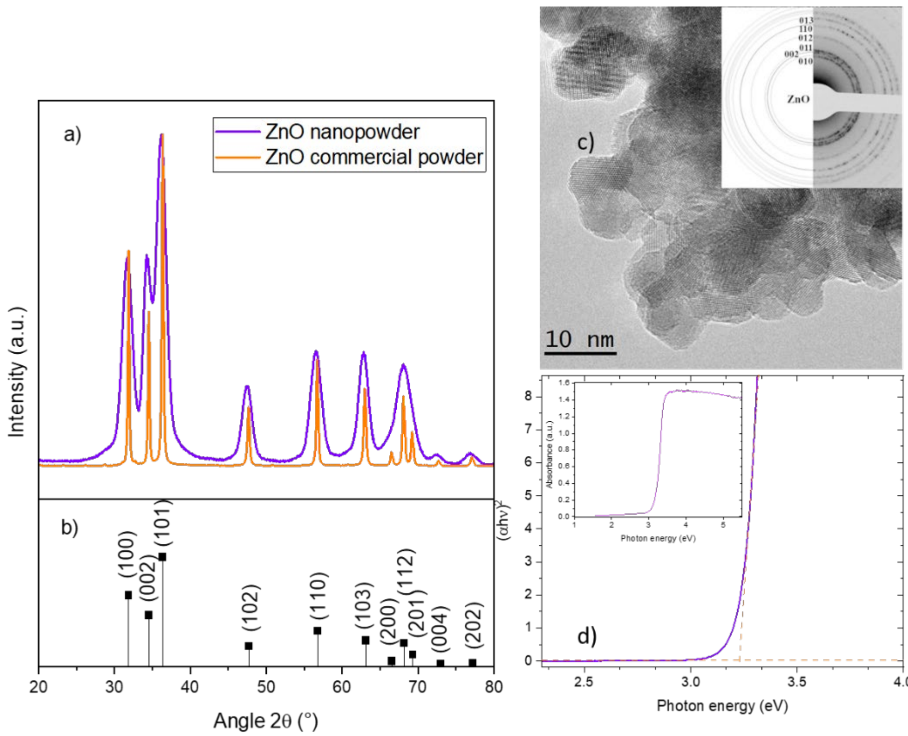

Figure 1: a) X-ray diffractograms of ZnO nanopowder (purple) and of ZnO commercial powder (orange). b) Theorical position of diffraction peaks of ZnO[28] c) HRTEM performed on ZnO nanopowder (measured and calculated diffraction patterns on inset) d) Tauc plot of ZnO nanopowder (UV-VIS absorption spectra on inset)

By using this relation, we can obtain an average crystallite size of 5.9 ± 0.5 nm. Furthermore, in order to verify if there is a correspondence between the crystallites size and the grain size, the ZnO NPs were analyzed by transmission electron microscopy.

The high-resolution images (Figure 1.c.) reveal that our nanoparticles exhibit primarily a round-shape microstructure. The alignments visible in the image cover the totality of the particles indicating the absence of any amorphous phase and a good surface crystallinity. The diffraction patterns obtained on these nanoparticles (Figure 1.c. in inset) agree with wurtzite ZnO structure. In addition, the NPs appear to be formed of a single crystallographic domain whose average grain size is 6.6 nm (measurement analysis conducted on two hundred grains with a standard deviation of 1 nm in accordance with the results obtained by the Scherrer's relation used in XRD). The ZnO nanopowder is also characterized by UV-VIS spectroscopy (Figure 1.d). We observe the presence of an absorption band near 3 eV and by plotting a Tauc plot (i.e. $(\alpha h\nu)^2$ versus $h\nu$ for a direct band gap [29], where α represent the absorption coefficient), we were able to determine the optical band gap situated at 3.23 eV. This value is in good agreement with measurements found in the literature for ZnO nanoparticles [30,31] and confirm the absorption of this material in the UV range.

In the next step, this powder was blended with liquid crystal. To do so, and to achieve proper dispersion of the nanoparticles within a liquid crystal medium, the ZnO nanopowder was first blended with oleic acid, serving as a surfactant[32], and in toluene serving as a solvent, following a mass ratio of 1:2:30 respectively. Subsequently, to achieve good dispersion, the suspension of coated ZnO nanoparticles in toluene was placed in a Fisher Scientific sonicator for one hour, resulting in the formation of a stable suspension that remained viable for up to one day without visible changes. Finally, this suspension was added in a nematic liquid crystal (1-(trans-4-Hexylcyclohexyl)-4-isothiocyanatobenzene, 6CHBT, Aldrich) with different weight percentage of

ZnO NPs in liquid crystals (1%, 3% and 10 %), and the toluene solvent was slowly evaporated from the mixture. The blend of ZnO NPs and liquid crystal was finally used to fill liquid crystal cells.

3.2 Investigation of electro-optical and photoelectrochemical properties of liquid crystal doped with ZnO nanoparticles

Commercial planar liquid crystal cells (Instec) with a gap of 5 µm were filled with different suspension of 6CHBT liquid crystal doped with ZnO nanoparticles functionalised by oleic acid surfactant. Polarized images and electro-optical curves recorded on these samples are presented on Figure 4.

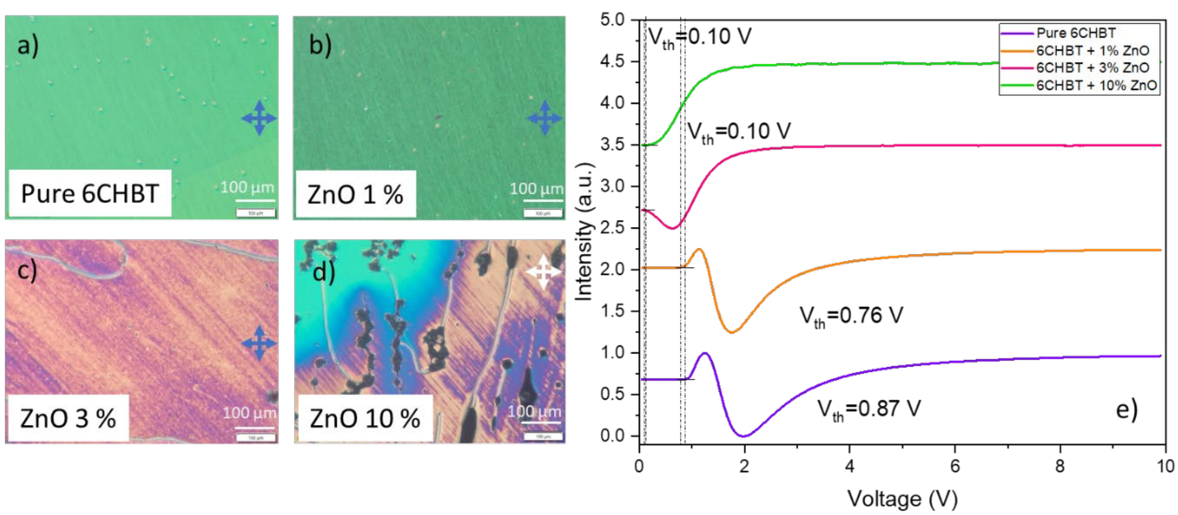

Figure 2 : Polarized optical microscopy images performed on planar liquid crystal cells filled with a) pure 6CHBT b) 6CHBT + 1 wt% ZnO nanoparticles c) 6CHBT + 3 wt% ZnO nanoparticles c) 6CHBT + 10 wt% ZnO nanoparticles e) Electro-optical curves recorded on pure and doped liquid crystal cells in parallel polarizers configuration.

One can note that Polarized Optical Microscopy (POM) images recorded on pure liquid crystal and on the liquid crystal doped with 1 wt% of ZnO NPs look similar and we did not observe the presence of aggregates or defects induced by the presence of nanoparticles. In reference to the sample containing 3 wt% of ZnO, notable alterations were observed. Specifically, the colour of the image acquired through polarized optical microscopy markedly differs from that obtained for both pure 6CHBT and 6CHBT doped with 1 wt% of ZnO. In this case, substantial colouration can be observed, falling within a spectrum ranging from orange to pink. Furthermore, we have identified the presence of several, distinct nematic defect lines. However, from macroscopic point of view, the overall alignment of liquid crystal molecules remained uniform. Finally, the cell filled with the suspension which contains 10 wt% of ZnO was significantly changed as compared to the undoped liquid crystal cell: we note the presence of several defect lines and the presence of black areas. The latter can be assigned to either homeotropic or isotropic domains. It is worth to note that all cells were filled after the total evaporation of the solvent and that the black domains were not created by the presence of a solvent. This modification of the alignment at high concentration of nanoparticles can be explained by a change of the pretilt angle caused by the accumulation of nanoparticles at the surface of alignment layers.

The electro-optical (EO) characteristics of these cells were measured by using standard, cross-polarised intensity setup[17] which was composed of two parallel polarisers, a He-Ne Laser, an AC generator and a photodetector connected to a computer. The angle between the polariser and the rubbed direction of polymer layer in the LC cell was fixed to 45°. The Freedericksz transition (i.e., the threshold voltage or V_{TH}) was estimated by the voltage which allows the first change in the transmitted light. The results are presented in Figure 3 e). First, we note that the EO curves obtained for the pure 6CHBT and for 6CHBT doped with 1% of ZnO are similar, but on closer inspection, a small decrease of the Freedericksz transition can be observed. The threshold voltage is given by

$$V_{th} = \pi\sqrt{\frac{K_1}{\varepsilon_0 \Delta\varepsilon}}$$

Equation 1

where K_1 and $\Delta\varepsilon$ are, respectively, the splay elastic constant and the dielectric anisotropy of the LC. The V_{TH} changes from 0.87 V for the pristine sample to 0.76 V for the doped sample. In the case of liquid crystal doped by ferroelectric nanoparticles ($BaTiO_3$[17], $Sn_2P_2S_6$[33]) this decrease was usually attributed to the coupling of the director (i.e., the mean orientation of LC molecules) and the polarisation of the nanoparticles or to the increase of the dielectric anisotropy due to the presence of the nanoparticles. The same decrease was observed by Sharma et al.[34] in the case of ZnO nanoparticles dispersed in E7 nematic liquid crystal. They attempted to elucidate this phenomenon by attributing it to two main factors: the field screening effects resulting from the presence of impurity ions, and the larger size of nanoparticles (NPs) compared to liquid crystal (LC) molecules, leading to a stronger dipole moment in NPs than in LCs. This increased dipole moment in NPs generates a strong electric torque, which influences the anchoring conditions and could potentially lead to a reduction in the threshold voltage[32]. Concerning the samples doped with higher concentration of ZnO (3% and 10%), we note a significant change in the EO curve. The Freedericksz threshold was difficult to measure reliably but could be estimated as 0.1 V for both samples. For these samples, the reduction in the threshold can be attributed to strong alterations in anchoring conditions induced by the presence of ZnO nanoparticles.

Photocurrent measurements using an optical chopper were done (Figure 3.a) on liquid crystal doped with ZnO (0.23 %, without surfactant) under different wavelengths (450 nm, 470 nm, 505 nm, 530 nm, 590 nm), under different power and under a bias of 1.5 V. Despite of the lack of surfactant, POM done on this sample do not show the presence of aggregates. We notice the presence of a photocurrent only when the shutter was open, and that the photocurrent falls quickly to zero when the shutter was closed. In addition, one can observe the presence of transient photocurrent when the shutter is open. This immediate photoresponse, consisting of an spike and followed by an exponential decay, can be explained by the separation [35] of photogenerated electron–hole pairs at the semiconductor/liquid crystal interface. The more detailed discussion of the time response will be presented in the next section, but here we focus on the strength of the photocurrent generated. In absence of incident light, the photocurrent approaches zero, indicating the fundamental thermodynamic state of the electrodes. In addition, we also note that despite the presence of the polyimide alignment layers in the liquid crystal cells, which can block the electron motion, we were able to measure a photocurrent in all doped liquid crystals cells. Under illumination, we detected a photo-generated current, a characteristic feature of n-type semiconductors, as documented in literature [36]. In addition, it is worth noting that a photocurrent is consistently measurable in all doped LC cells when illuminated, a phenomenon notably absent in LC cells filled with pure LC, whatever the applied bias voltage or light intensity levels. Furthermore, while the maximum photocurrent response was obtained for the incident 450 nm light beam, a photoresponse could also be detected up to 500 nm. However, with the current setup, it was not possible to measure the photocurrent for longer wavelengths. These observations show that such hybrid ZnO-LC device can be a good candidate to serve in multispectral photodetector applications [10]. Finally, we observed a strong decrease of the photocurrent with the wavelength increase (Figure 3.b). This evolution follows the decrease of the absorbance of ZnO nanoparticles (band-gap at 3.23 eV (383 nm)) with the wavelength obtained on figure 1d and is in good agreement with the trends reported in the literature [37] .

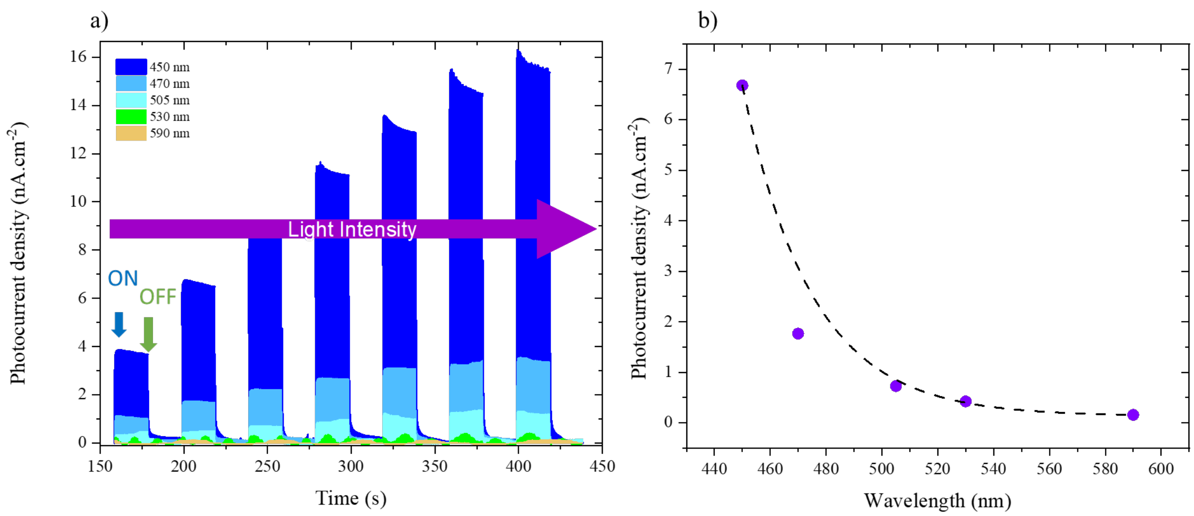

Figure 3: a) Photocurrent measurements using chopped light done on doped liquid crystal cell (0.23%w/w ZnO, without surfactant) under a light with variable light power density (from 11 mW.cm^{-2} to 120 mW.cm $^{-2}$ at 450 nm ; from 17 mW.cm^{-2} to 74 mW.cm^{-2} at 470 nm ; from 15 mW.cm^{-2} to 58 mW.cm $^{-2}$ at 505 nm ; from 17 mW.cm^{-2} to 36 mW.cm $^{-2}$ at 530 nm ; from 13 mW.cm^{-2} to 53 mW^{-2} at 590 nm) and under a bias of 1.5 V b) Evolution of the maximum photocurrent with the wavelength of the light sources for a light power density at 33 mW.cm^{-2}.

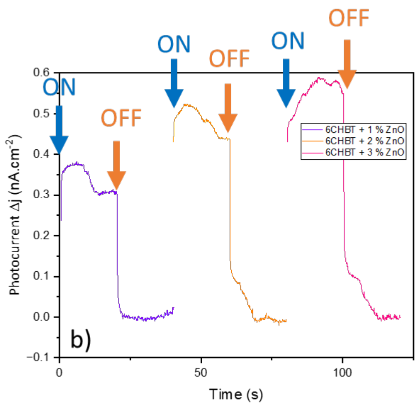

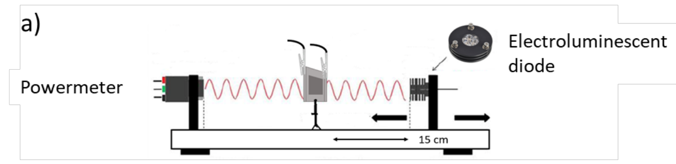

c)	τ_r (s)	τ_d (s)	Photocurrent density (Δj = nA.cm^{-2})
ZnO 1 %	0.27	0.24	0.31
ZnO 2 %	0.32	0.28	0.44
ZnO 3 %	0.32	0.37	0.55

Figure 4: a) Chronoamperometric measurements done on doped liquid crystal cells under a light at 450 nm and with a power density of 75 mW.cm^{-2} and under a bias of 1.5 V. c) Table of results including response and recovery times and maximum photocurrents density for the three doped cells.

Photocurrent measurements were also realized on liquid crystals cells doped with 1% ZnO, 2% ZnO and 3% ZnO (Figure 4). In this part, the nanoparticles were covered with oleic acid to improve their dispersion and stability in the liquid crystal matrix. First, it can be observed that the value of the photocurrent density increased with the concentration of nanoparticles in the liquid crystal. Secondly, the photocurrent was lower than the photocurrent obtained in the case of the nanoparticles dispersed without surfactant (Figure 3). For the three concentrations of ZnO, we determined the values of the response τ_r and recovery τ_d times of all cells given by $\tau_r = t_{90\%}\text{-}t_{10\%}$ and $\tau_d = t_{10\%}\text{-}t_{90\%}$, where $t_{10\%}$ and $t_{90\%}$ represent the time at 10% and 90% of the maximum value of the photocurrent. It is worth highlighting that both of these response times are close to 0.3 s and, are closed to the responses times found in the literature for the case of ZnO photodetectors [38].

This is a very encouraging result that demonstrates that our system can be used as fast and embedded photodetector in liquid crystal devices, including various displays.

The weakest photocurrent densities obtained in some cases can be explained through the following, several mechanisms. The highest concentration of ZnO NPs in the LC cell can induce defects in the liquid crystal cell and thus reduce the photocurrent. The wavelength of our electroluminescent diode was not completely tuned to the wavelength of the optical band gap of ZnO and the decreased yield of the photocurrent production can be expected. The presence of surfactant molecules at the surface of nanoparticles, and the presence of polyimide alignment layer in the LC cells, while essential to provide a good dispersion of NPs and a good LC alignment quality respectively, can limit the photocurrent by capturing the charge carriers.

In the next part we will evaluate the influence of the presence of the surfactant on the value of the photocurrent.

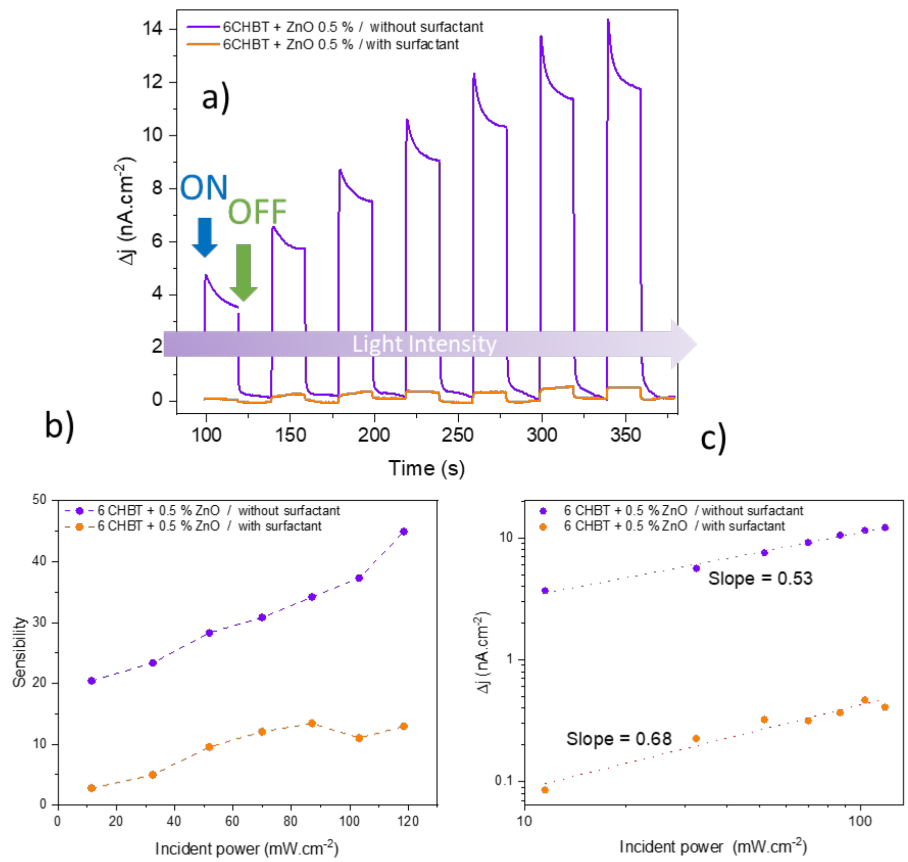

Figure 5: a) Light measurements with optical chopper performed on doped liquid crystal cells under a light at 450 nm and with a variable light power density (from 11 $mW.cm^{-2}$ to 120 $mW.cm^{-2}$) and under a bias of 1.5 V. b) Evolution of the sensibility of doped cells with the power density of light c) Evolution of the maximum photocurrent density of doped cells with incident power of light in log-log graph.

Figure 5.a presents the comparison of electrochemical curves (photocurrents evolution with time) recorded on samples containing ZnO covered with or without surfactant (oleic acid). We can remark that the measured photocurrent is 20 to 30 times higher for cells with uncoated ZnO NPs, compared to those with ZnO coated with surfactant. This strong trend confirms the mechanism of

trapping of photo-charge carriers by surfactant molecules present at the surface of nanoparticles. In spite of not perfectly uniform dispersion of the nanoparticles, and the possible presence of aggregates, the absence of ligand improves significantly the photocurrent harvesting. In figure 4.b and 4.c, we present the evolution of the sensitivity (j_{light}/j_{dark}) and the mean steady-state photocurrent density of both samples in log-log diagram. First, we can note that the sensitivity is always higher without the presence of the surfactant molecules and shows the degradation of photocurrent generation caused by these molecules. Indeed, is it well known that the evolution of the photocurrent can be described by a steady-state rate equation[39],

G=Bn(n+M) Equation 2

Where G is the generation rate of the photoelectrons by the incident light, B is the recombination coefficient, n is the density of photoelectrons and M represent the density of impurities.

In the case of low light intensity, the density of photoelectrons is lower than the density of impurities and we obtain the following relation n=G/(BM). As $I_{PC} \propto n$ (I_{PC} is the intensity of the photocurrent) and $G \propto I_{in}$ (I_{in} is the light intensity), we can conclude that the intensity of the photocurrent follows a linear relation with the incident light intensity $I_{PC} \propto I_{in}$. However, when the light intensity is increased, or, in the case of low impurities, we obtain the following relation $n^2 = \frac{G}{B}$ and we can conclude that the photocurrent follows the relation $I_{PC} \propto (I_{in})^{0.5}$.

In figure 5.c, we used a log-log graph to represent the evolution of the photocurrent with the incident light intensity and we perform a linear fitting in order to find the exponent in the power law $I_{PC} \propto (I_{in})^{s}$. We note a slope of 0.53 in the case of nanoparticles without ligands and 0.68 in the case of nanoparticles surrounding with surfactants molecules. As we used moderate light intensity, we can conclude that the ZnO nanoparticles without surfactant behaviour is similar to a semiconductor material without impurities [39]. The small increase of the slope in the case of nanoparticles functionalised with surfactant molecules can be interpreted as an effective increase of impurities of the material cause by the presence of these molecules.

4. CONCLUSION

High purity ZnO nanoparticles were successfully synthetized and characterized with average diameters of about 6 nm and without any trace of amorphization. When incorporated into a nematic liquid crystal medium, the nanoparticles lead to a remarkable photocurrent response, detectable across a broad spectrum up to 500 nm and with response times (300 ms) closed to the best values found in the literature for ZnO photodetectors. Furthermore, we demonstrated the enhancement of the photocurrent (up to 30 times) when nanoparticles are not functionalized with a surfactant. Analysis of photocurrent with the incident light power suggests that surfactant-free hybrid liquid crystal behaves similarly to a material with minimal impurities. However, the presence of surfactant molecules appears to increase the concentration of impurities, affecting the photocurrent generation. This study suggests that future research on optimizing surfactant type and concentration could improve nanoparticles dispersion without compromising photocurrent generation. This improvement offers promising implications for the seamless integration of photodetectors into liquid crystal devices, particularly for liquid crystal displays. The results presented here not only offer valuable knowledge on ZnO nanoparticles, but also hold significant promise for the development of high-performance, liquid crystal-based photodetection technology.

Acknowledgement:

This work was partially supported by the "PHC Alliance" programme (project number: 47835NK), funded by the French Ministry for Europe and Foreign Affairs, the French Ministry for Higher Education and Research and the UK British Council. The authors thank the CPER MANIFEST for its financial support.

References

[1] H. Kaushal, G. Kaddoum, Optical Communication in Space: Challenges and Mitigation Techniques, IEEE Commun. Surv. Tutorials 19 (2017) 57–96. https://doi.org/10.1109/COMST.2016.2603518.

[2] J.L. Pau, J. Anduaga, C. Rivera, Á. Navarro, I. Álava, M. Redondo, E. Muñoz, Optical sensors based on III-nitride photodetectors for flame sensing and combustion monitoring, Appl. Opt. 45 (2006) 7498–7503. https://doi.org/10.1364/AO.45.007498.

[3] A. Puga, A. Yalin, Ozone Detection via Deep-Ultraviolet Cavity-Enhanced Absorption Spectroscopy with a Laser Driven Light Source, Sensors 23 (2023). https://doi.org/10.3390/s23114989.

[4] S. Sivaraj, R. Rathanasamy, G.V. Kaliyannan, H. Panchal, A. Jawad Alrubaie, M. Musa Jaber, Z. Said, S. Memon, A Comprehensive Review on Current Performance, Challenges and Progress in Thin-Film Solar Cells, Energies 15 (2022). https://doi.org/10.3390/en15228688.

[5] R. Soleimanzadeh, M. Kolahdouz, M.A. Charsooghi, Z. Kolahdouz, K. Zhang, Highly selective and responsive ultra-violet detection using an improved phototransistor, Appl. Phys. Lett. 106 (2015) 3–5. https://doi.org/10.1063/1.4922638.

[6] L. Goswami, N. Aggarwal, P. Vashishtha, S.K. Jain, S. Nirantar, J. Ahmed, M.A.M. Khan, R. Pandey, G. Gupta, Fabrication of GaN nano-towers based self-powered UV

photodetector, Sci. Rep. 11 (2021) 1–10. https://doi.org/10.1038/s41598-021-90450-w.

[7] Z. Li, Z. Li, C. Zuo, X. Fang, Application of Nanostructured TiO2 in UV Photodetectors: A Review, Adv. Mater. 34 (2022) 1–43. https://doi.org/10.1002/adma.202109083.

[8] Q. Liao, C. Mu, D.-S. Xu, X.-C. Ai, J.-N. Yao, J.-P. Zhang, Gold nanorod arrays with good reproducibility for high-performance surface-enhanced Raman scattering., Langmuir 25 (2009) 4708–14. https://doi.org/10.1021/la8036555.

[9] H. Ferhati, F. Djeffal, A. Bendjerad, L. Foughali, A. Benhaya, A. Saidi, sputtered amorphous SiC thin-film : Effect of sputtering power, J. Alloys Compd. 907 (2022) 164464. https://doi.org/10.1016/j.jallcom.2022.164464.

[10] E. Nurfani, M.A.K. Purbayanto, T. Aono, K. Takase, Y. Darma, Origin of fast-response photocurrent in ZnO thin film, Opt. Mater. (Amst). 84 (2018) 453–458. https://doi.org/10.1016/j.optmat.2018.07.040.

[11] Z.Y. Xue, D.H. Zhang, Q.P. Wang, J.H. Wang, The blue photoluminescence emitted from ZnO films deposited on glass substrate by rf magnetron sputtering, Appl. Surf. Sci. 195 (2002) 126–129. https://doi.org/10.1016/S0169-4332(02)00547-0.

[12] M. Kumar, S. Kumar, Liquid crystals in photovoltaics: A new generation of organic photovoltaics, Polym. J. 49 (2017) 85–111. https://doi.org/10.1038/pj.2016.109.

[13] H.K. Bisoyi, Q. Li, Liquid Crystals: Versatile Self-Organized Smart Soft Materials, Chem. Rev. 122 (2022) 4887–4926. https://doi.org/10.1021/acs.chemrev.1c00761.

[14] Z. Rouhbakhsh, J.W. Huang, T.Y. Ho, C.H. Chen, Liquid crystal-based chemical sensors and biosensors: From sensing mechanisms to the variety of analytical targets, TrAC - Trends Anal. Chem. 157 (2022) 116820. https://doi.org/10.1016/j.trac.2022.116820.

[15] M. Kumar, S. Kumar, Liquid crystals in photovoltaics: A new generation of organic

photovoltaics, Polym. J. 49 (2017) 85–111. https://doi.org/10.1038/pj.2016.109.

[16] R. Dabrowski, P. Kula, J. Herman, High birefringence liquid crystals, 2013. https://doi.org/10.3390/cryst3030443.

[17] J.F. Blach, S. Saitzek, C. Legrand, L. Dupont, J.F. Henninot, M. Warenghem, BaTiO3 ferroelectric nanoparticles dispersed in 5CB nematic liquid crystal: Synthesis and electro-optical characterization, J. Appl. Phys. 107 (2010). https://doi.org/10.1063/1.3369544.

[18] O. Kurochkin, E. Mavrona, V. Apostolopoulos, J.-F. Blach, J.-F. Henninot, M. Kaczmarek, S. Saitzek, M. Sokolova, Y. Reznikov, Electrically charged dispersions of ferroelectric nanoparticles, Appl. Phys. Lett. 106 (2015) 043111. https://doi.org/10.1063/1.4907224.

[19] E. Mavrona, U. Chodorow, M.E. Barnes, J. Parka, N. Palka, S. Saitzek, J.-F. Blach, V. Apostolopoulos, M. Kaczmarek, Refractive indices and birefringence of hybrid liquid crystal - Nanoparticles composite materials in the terahertz region, AIP Adv. 5 (2015). https://doi.org/10.1063/1.4927392.

[20] L.J. Martínez-Miranda, K.M. Traister, I. MeÍndez-Rodríguez, L. Salamanca-Riba, Liquid crystal-ZnO nanoparticle photovoltaics: Role of nanoparticles in ordering the liquid crystal, Appl. Phys. Lett. 97 (2010) 6–9. https://doi.org/10.1063/1.3511736.

[21] A. Meneses-Franco, A.E. Fierro-Armijo, P. Romero-Hasler, L.G. Salamanca-Riba, L.J. Martínez-Miranda, E.A. Soto-Bustamante, Smectogenic liquid crystals and nanoparticles: An approach for potential application in photovoltaics, J. Mater. Chem. C 3 (2015) 8566–8573. https://doi.org/10.1039/c5tc00482a.

[22] L.J. Martínez-Miranda, J.W. Taylor, L.K. Kurihara, Liquid Crystals Nanocomposites for Photovoltaic Applications: Structural Properties, Mol. Cryst. Liq. Cryst. 594 (2014) 100–104. https://doi.org/10.1080/15421406.2014.917495.

[23] L. Spanhel, M.A. Anderson, Semiconductor Clusters in the Sol-Gel Process: Quantized Aggregation, Gelation, and Crystal Growth in Concentrated ZnO Colloids, J. Am. Chem. Soc. 113 (1991) 2826–2833. https://doi.org/10.1021/ja00008a004.

[24] E.A. Meulenkamp, Synthesis and Growth of ZnO Nanoparticles, J. Phys. Chem. B 102 (1998) 5566–5572. https://doi.org/10.1021/jp980730h.

[25] A. Glaria, M.L. Kahn, T. Cardinal, F. Senocq, V. Jubera, B. Chaudret, Lithium ion as growth-controlling agent of ZnO nanoparticles prepared by organometallic synthesis, New J. Chem. 32 (2008) 662–669. https://doi.org/10.1039/b715583b.

[26] L.P. Brazuna, T.G. Tabuti, A.D.P. Silva, D.B. Tada, M.J. Politi, R. Bacani, E.R. Triboni, Effect of lithium and sodium ions on the size and morphology of ZnO nanoparticles synthesized by a glycerol-urea route, New J. Chem. 43 (2019) 18988–18995. https://doi.org/10.1039/c9nj04331d.

[27] A.L. Patterson, The scherrer formula for X-ray particle size determination, Phys. Rev. 56 (1939) 978–982. https://doi.org/10.1103/PhysRev.56.978.

[28] S.C. Abrahams, J.L. Bernstein, Remeasurement of the structure of hexagonal ZnO, Acta Crystallogr. Sect. B Struct. Crystallogr. Cryst. Chem. 25 (1969) 1233–1236. https://doi.org/10.1107/s0567740869003876.

[29] W. R. Saleh, N. M. Saeed, W. A. Twej, M. Alwan, Synthesis Sol-Gel Derived Highly Transparent ZnO Thin Films for Optoelectronic Applications, Adv. Mater. Phys. Chem. 02 (2012) 11–16. https://doi.org/10.4236/ampc.2012.21002.

[30] S. Agarwal, L.K. Jangir, K.S. Rathore, M. Kumar, K. Awasthi, Morphology-dependent structural and optical properties of ZnO nanostructures, Appl. Phys. A Mater. Sci. Process. 125 (2019) 1–7. https://doi.org/10.1007/s00339-019-2852-x.

[31] S.K. Mishra, R.K. Srivastava, S.G. Prakash, Photoluminescence and photoconductivity studies of ZnO nanoparticles prepared by solid state reaction method, J. Mater. Sci. Mater. Electron. 24 (2013) 125–134. https://doi.org/10.1007/s10854-012-0950-z.

[32] N. Podoliak, O. Buchnev, M. Herrington, E. Mavrona, M. Kaczmarek, A.G. Kanaras, E. Stratakis, J.-F. Blach, J.-F. Henninot, M. Warenghem, Elastic constants, viscosity and response time in nematic liquid crystals doped with ferroelectric nanoparticles, RSC Adv. 4 (2014) 46068–46074. https://doi.org/10.1039/C4RA06248E.

[33] N. Podoliak, O. Buchnev, M. Herrington, E. Mavrona, M. Kaczmarek, A.G. Kanaras, E. Stratakis, J.F. Blach, J.F. Henninot, M. Warenghem, Elastic constants, viscosity and response time in nematic liquid crystals doped with ferroelectric nanoparticles, RSC Adv. 4 (2014) 46068–46074. https://doi.org/10.1039/c4ra06248e.

[34] A. Sharma, P. Malik, R. Dhar, P. Kumar, Improvement in electro-optical and dielectric characteristics of ZnO nanoparticles dispersed in a nematic liquid crystal mixture, Bull. Mater. Sci. 42 (2019). https://doi.org/10.1007/s12034-019-1902-5.

[35] L.M. Peter, A.B. Walker, T. Bein, A.G. Hufnagel, I. Kondofersky, Interpretation of photocurrent transients at semiconductor electrodes: Effects of band-edge unpinning, J. Electroanal. Chem. 872 (2020) 114234. https://doi.org/10.1016/j.jelechem.2020.114234.

[36] E.P. Mukhokosi, G.V.S. Manohar, T. Nagao, S.B. Krupanidhi, K.K. Nanda, Device architecture for visible and near-infrared photodetectors based on two-dimensional SnSe2 and MoS2: A review, Micromachines 11 (2020) 1–30. https://doi.org/10.3390/MI11080750.

[37] S.K. Mishra, R.K. Srivastava, S.G. Prakash, R.S. Yadav, A.C. Panday, Photoluminescence and photoconductive characteristics of hydrothermally synthesized ZnO nanoparticles, Opto-Electronics Rev. 18 (2010) 467–473. https://doi.org/10.2478/s11772-010-0037-4.

[38] B. Deka Boruah, Zinc oxide ultraviolet photodetectors: Rapid progress from conventional to self-powered photodetectors, Nanoscale Adv. 1 (2019) 2059–2085. https://doi.org/10.1039/c9na00130a.

[39] B. Ullrich, H. Xi, Photocurrent limit in nanowires, Opt. Lett. 38 (2013) 4698. https://doi.org/10.1364/ol.38.004698.